

Calibration of the high-frequency magnetic fluctuation diagnostic in plasma devices

L. C. Appel and M. J. Hole

Citation: [Review of Scientific Instruments](#) **76**, 093505 (2005); doi: 10.1063/1.2009107

View online: <http://dx.doi.org/10.1063/1.2009107>

View Table of Contents: <http://scitation.aip.org/content/aip/journal/rsi/76/9?ver=pdfcov>

Published by the [AIP Publishing](#)

Articles you may be interested in

[A real-time algorithm for the harmonic estimation and frequency tracking of dominant components in fusion plasma magnetic diagnostics](#)

Rev. Sci. Instrum. **84**, 083508 (2013); 10.1063/1.4818967

[In situ “artificial plasma” calibration of tokamak magnetic sensors](#)

Rev. Sci. Instrum. **84**, 063502 (2013); 10.1063/1.4808366

[Localized measurement of short wavelength plasma fluctuations with the DIII-D phase contrast imaging diagnostic](#)

Rev. Sci. Instrum. **80**, 023503 (2009); 10.1063/1.3065094

[Characterization of coherent magnetic fluctuations in JFT-2M high recycling steady high-confinement mode plasmas](#)

Phys. Plasmas **13**, 032507 (2006); 10.1063/1.2169779

[Fast magnetic fluctuation diagnostics for Alfvén eigenmode and magnetohydrodynamics studies at the Joint European Torus](#)

Rev. Sci. Instrum. **71**, 4092 (2000); 10.1063/1.1313797

Nor-Cal Products



Manufacturers of High Vacuum
Components Since 1962

- Chambers
- Motion Transfer
- Flanges & Fittings
- Viewports
- Foreline Traps
- Feedthroughs
- Valves



www.n-c.com
800-824-4166

Calibration of the high-frequency magnetic fluctuation diagnostic in plasma devices

L. C. Appel^{a)}

Euratom/UKAEA Fusion Association, Culham Science Centre, Abingdon, Oxfordshire, OX14 3DB, United Kingdom

M. J. Hole

Department of Theoretical Physics and Plasma Research Laboratory, Australian National University, Canberra, A.C.T. 0200, Australia

(Received 22 November 2004; accepted 18 April 2005; published online 9 September 2005)

The increasing reservoirs of energetic particles which drive high-frequency modes, together with advances in the understanding of magnetohydrodynamics, have led to a need for higher-frequency (50 kHz to >20 MHz) measurements of magnetic field fluctuations in magnetic fusion devices such as tokamaks. This article uses transmission line equations to derive the voltage response of a Mirnov coil at the digitizer end of a transmission line of length ℓ . It is shown that, depending on the terminations of the line, resonances can occur even for $\ell/\lambda \ll 1$, with λ the wavelength of a fluctuation in the transmission line. A lumped-circuit model based on the approach of Heeter *et al.* [R. F. Heeter, A. F. Fasoli, S. Ali-Arshad, and J. M. Moret. *Rev. Sci. Instrum.* **71**, 4092 (2000)] is extended to enable the inclusion simultaneously of both serial resistance and parallel conductance elements. As originally proposed by Heeter *et al.* the lumped-circuit model offers the advantage of remote calibration; this may be of particular value when upgrading existing systems to operate at frequencies above the original design specification. It is formally shown that the transmission line equations for the transfer function and measured impedance reduce to those of the lumped circuit model of Heeter *et al.* under specific conditions. The result extends the use of the lumped-circuit model of Heeter *et al.*, which can be used to extract the transfer function from measurement of the impedance, beyond the case of an open-circuit termination. Although the numerical procedure does exhibit some problems associated with non-uniqueness, it provides a simple calibration method for systems that are not well defined. Using typical parameters for a high-frequency Mirnov coil installed on the Joint European Torus (JET) tokamak, the lumped-circuit approximation agrees with the steady-state transmission line model to within 0.015° in phase and 22% in amplitude for frequencies up to 1 MHz. A matched termination, though eliminating line resonances and reducing the length of time for the system to reach steady state, is inappropriate for the JET-type coils which exhibit significant temperature-dependent resistance. Finally, for fluctuations of finite duration, a method of computing the discrepancy due to the simplifying assumption of Fourier-stationary conditions is described. © 2005 American Institute of Physics. [DOI: 10.1063/1.2009107]

I. INTRODUCTION

The increasing energetic particle populations responsible for driving high-frequency modes in magnetic fusion devices such as tokamaks, and accompanying advances in the understanding of magnetohydrodynamics have led to a need for measurements of magnetic field fluctuations at higher frequencies in the range 50 kHz to >20 MHz. In many of these devices there is a large base of installed hardware which was designed mainly for low-frequency measurements. Often, the design and installation of entirely new systems is cost prohibitive, and the most feasible approach to high-frequency measurements is to simply upgrade the digitizers on the older hardware. In either the new-system or upgraded-system situations, the issue of high-frequency calibration is a major

challenge, especially for ongoing operations, since the diagnostics on many devices are essentially inaccessible after installation. This article provides some important insights into this issue.

Magnetic fluctuations well above 100 kHz driven by energetic particles are now commonly observed on tokamaks with auxiliary heating. Types of activity reported include shear Alfvén modes, for example, the toroidal and elliptical Alfvén eigenmodes,^{1–3} formed in gaps of the continuous Alfvén spectrum in which $f = k_{\parallel} v_A / 2\pi$, ion cyclotron eigenmodes (ICE)⁴ and compressional Alfvén eigenmodes (CAEs)⁵ with $f = |k| v_A / 2\pi$. Here k denotes the mode wave number (k_{\parallel} is the component orientated with the magnetic field) and v_A is the local Alfvén velocity. For the normal operating conditions in tokamaks, it is expected that these instabilities should have frequencies in the range 50–400 kHz for shear Alfvén eigenmodes and extending up to above the cyclotron frequency for CAEs [~ 4 MHz in the Mega-

^{a)} Author to whom correspondence should be addressed; electronic mail: lynton.appel@ukaea.org.uk

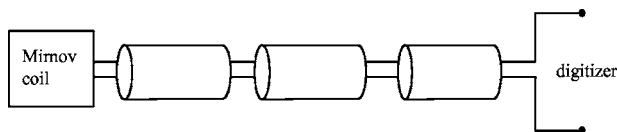


FIG. 1. Schematic diagram showing the Mirnov coil connected via a number of separate transmission line sections (three are shown in the figure) to a digitizer.

Amp Spherical Tokamak (MAST) and the National Spherical Torus Experiment (NSTX), and ~ 20 MHz in the Joint European Torus (JET)]. Experimental measurements have confirmed these values. Shear Alfvénic activity has been seen on JET around 250 kHz,⁶ on MAST up to 400 kHz,⁷ and on the Small Tight Aspect Ratio Tokamak (START) between 50 and 350 kHz.⁸ Evidence of CAEs and ICE have been seen on JET,⁹ START,⁸ NSTX¹⁰ and more recently on MAST.¹¹

The simplest technique for the detection of magnetic field fluctuations is by the use of magnetic Mirnov probes.¹² Modern experimental practice is to connect the probes via a twisted wire or coaxial cable to a digitizer. Due to the stringent operating conditions within the vacuum vessel, the electrical properties of the cables used inside the vessel and outside the vessel are not necessarily the same; also, in some cases the distance between the vessel and the digitizer may be connected with multiple cables again with varying electrical properties. Generally, the inhomogeneity of the cables only becomes important at higher frequencies due to transmission line effects. Figure 1 shows a schematic diagram of the circuit from the Mirnov coil to the digitizer. Although Mirnov probes have been in use for many years, the focus has been mainly on the detection of frequencies below 50 kHz where the effect of the connecting cable may be neglected or at most be included as an effective capacitance.¹³ The possibility of resonances at low frequencies between the line capacitance and probe inductance was recognized by Lovberg¹⁴ in the early 1960s. Published analysis techniques range from a complete neglect of line effects¹⁵ to considering only the phase delays in the line.¹⁶ In the work of Heeter *et al.*¹⁷ steady-state transmission line effects are taken into account in an approximate manner using a discrete lumped-circuit approach; they also describe an approach to the issue of in-vessel calibration.

While this work is motivated by recent advances in toroidal magnetic confinement, the techniques developed here have application to other *in situ* measurements in space and experimental plasmas. Magnetometers,¹⁸ which detect field strength and orientation, are typically slow time scale (< 1 ms) magnetic probes, used extensively in satellites. While the variation in the detected field strength is often attributable to changes in the local plasma properties (e.g., density, temperature and flow speed), wave phenomena have also been detected.¹⁹ In low-temperature low-pressure inductively coupled plasmas, magnetic probes have been used to map the B field spatial variation at the fundamental and harmonics of the 0.5 MHz excitation frequency.²⁰ Magnetic fluctuation probes, also known as “B-dot” probes, have also been used in vacuum arc rail-gun experiments to characterize the expanding metal plasma plume.²¹ On faster-time scales

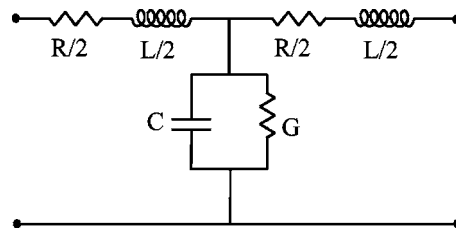


FIG. 2. A single T -model circuit.

($< 0.1 \mu\text{s}$), arrays of magnetic probes have been used to study the magnetohydrodynamics, stability of the imploding plasma in a Z pinch.²² Finally, on a very fast time scale (~ 1 ns), magnetic probes have been used to study the interaction of an externally applied magnetic field, a background plasma, and a laser-produced plasma.²³

In this work we apply transmission line theory to model the wave propagation from a Mirnov coil along a single terminated line. The analysis, valid for frequency-independent circuit parameters and steady-state conditions, elucidates the underlying physics. Extension of the theory to include the effects of using multiple cables is a straightforward generalization of the single cable case. Section II develops expressions for the voltage transfer function, the system impedance and the location of resonances. In Sec. III the lumped-circuit method of Heeter *et al.*¹⁷ is generalized to include resistive elements. Section IV examines the applicability of the lumped-circuit model when transmission line effects are included and shows that the model is valid providing that the transmission line is distortionless, and the load impedance real. For comparative purposes with the work of Heeter *et al.* calculations presented in this article are in the frequency range up to 1 MHz, however, it is valid to extend the frequency range far higher until the frequency dependences of the circuit parameters become significant. Finally, Sec. V examines the validity of the transmission line analysis in the case of finite-duration wave pulses.

II. TRANSMISSION LINE MODEL

Equations for the propagation of the voltage $V(z, t)$ and current $I(z, t)$ along a transmission line are described by the transmission-line equations²⁴

$$\frac{\partial V}{\partial z} = -\mathcal{L} \frac{\partial I}{\partial t} - IR, \quad (1)$$

$$\frac{\partial I}{\partial z} = -\mathcal{G}V - C \frac{\partial V}{\partial t}, \quad (2)$$

where \mathcal{L} , \mathcal{C} , \mathcal{R} , and \mathcal{G} are the transmission line parameters: inductance, capacitance, series resistance and parallel conductance per unit length of the transmission line in the z -direction, respectively. Alternatively, the transmission line may be represented by an infinite cascade of identical T -model circuit elements of the form shown in Fig. 2. The equivalent-circuit representation of the transmission lines shown in Fig. 1 consists of a separate infinite cascade of identical T -model circuits for each section of transmission line.

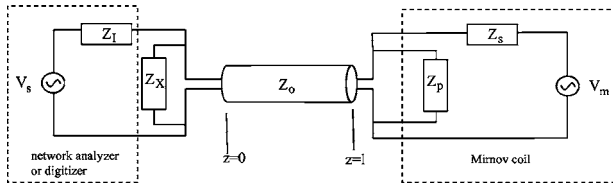


FIG. 3. Model of a transmission line showing details of the terminations at $z=0$ and $z=l$.

Instead of analyzing the electrical analog, we return to the transmission line equations (1) and (2) to examine wave propagation in a single transmission line section with terminations as shown in Fig. 3. At $z=0$ there is an arbitrary termination with impedance Z_X connected in parallel to a network analyzer represented by its Thévenin equivalent circuit:²⁵ an ideal voltage source V_s in series with an impedance Z_I . The network analyzer (for example, we have used a Rohde & Schwarz ZVRE vector network analyzer²⁶) has been included to enable calibration;¹⁷ in normal operation it is replaced by a high-impedance digitizer. Inclusion of the termination impedance Z_X allows adjustment of the wave boundary conditions at the input end. At $z=l$ there is a Mirnov coil represented by an ideal voltage source V_m , and the impedances $Z_S=R_p+j\omega L_p$ and $Z_P=1/j\omega C_p$ in which R_p, L_p and C_p are the resistance, inductance and stray capacitance,²⁷ respectively.

Below we consider the circuit characteristics of the cases when (a) $|V_s|>0, V_m=0$ (wave injected by the network analyzer), and (b) $|V_s|=0, Z_I=\infty, V_m>0$ (wave injected by Mirnov coil with network analyzer not present). In case (a) our analysis solves for both the voltage transfer function $T_s = V(z=l)/V_s$ between the end of the transmission line and the network analyzer, and the impedance seen by the network analyzer. In case (b) we solve the voltage transfer function $T_m = V(z=0)/V_m$ between the digitizer and the Mirnov coil.

Consider first the case of a wave injected by the network analyzer. Waves injected into the transmission line have current $I=\bar{I}\exp j\omega t$ and voltage $V=\bar{V}\exp j\omega t$ where ω is the wave frequency and \bar{I} and \bar{V} are the amplitudes of the voltage and current waves, respectively. Assuming the transmission line parameters are frequency-invariant, the system can be reduced to two coupled ordinary differential equations

$$\frac{d\bar{V}}{dz} = -(j\omega\mathcal{L} + \mathcal{R})\bar{I}, \quad (3)$$

$$\frac{d\bar{I}}{dz} = -(j\omega\mathcal{C} + \mathcal{G})\bar{V}, \quad (4)$$

which combined yield a wave equation for \bar{V}

$$\frac{d^2\bar{V}}{dz^2} = \gamma^2\bar{V}, \quad (5)$$

where $\gamma = \sqrt{(j\omega\mathcal{L} + \mathcal{R})(j\omega\mathcal{C} + \mathcal{G})}$ is the propagation constant of the wave. The *forward* wave solution for \bar{V} (i.e., the wave propagating in the positive z direction) is

$$\bar{V} = Ae^{-\gamma z} \quad (6)$$

with A an arbitrary integration constant. Substituting for \bar{V} in Eq. (3) yields

$$\bar{I} = \frac{Ae^{-\gamma z}}{Z_0}, \quad (7)$$

where $Z_0 = \sqrt{(j\omega\mathcal{L} + \mathcal{R})/(j\omega\mathcal{C} + \mathcal{G})}$ is the characteristic impedance of the transmission line. In terms of I and V

$$V = Ae^{j\omega t - \gamma z}, \quad (8)$$

$$I = \frac{A}{Z_0}e^{j\omega t - \gamma z} \quad (9)$$

and so the phase velocity of the wave is $v_{\text{phase}} = \omega/\text{Im}[\gamma]$. From these equations for V and I it is seen that the input impedance of the line encountered by a single wave propagating from the external source $V/I=Z_0$; hence

$$\frac{V_{(f,0,z=0)}}{V_s} = \frac{Z_0\|Z_X}{Z_0\|Z_X + Z_I}, \quad (10)$$

where $V_{(f,0,z=0)}$ is the forward propagating wave at $z=0$ with zero previous reflections and $X\|Y \equiv 1/(1/X + 1/Y)$.

A wave injected into the line by the network analyzer will in general be reflected multiple times, at $z=0$ and at $z=l$, and the net voltage and current will be a superposition of these waves. The voltage reflection coefficients²⁸ for a wave propagating towards $z=l$ and $z=0$ are

$$\Gamma_\ell = \frac{Z_P\|Z_S - Z_0}{Z_P\|Z_S + Z_0}, \quad (11)$$

$$\Gamma_0 = \frac{Z_I\|Z_X - Z_0}{Z_I\|Z_X + Z_0}, \quad (12)$$

respectively. At $z=0$, the forward and backward waves can be written as the summation of the number, n , of complete transits of the wave within the line. That is,

$$V_b(z=0) = \frac{V_{(f,0,z=0)}}{\Gamma_0} \sum_{i=0}^{n-1} (\Gamma_0\Gamma_\ell e^{-2\gamma\ell})^i, \quad (13)$$

$$V_f(z=0) = V_{(f,0,z=0)} \sum_{i=0}^{n-1} (\Gamma_0\Gamma_\ell e^{-2\gamma\ell})^i. \quad (14)$$

The total voltage appearing at $z=0$ and $z=l$ is obtained by summing the forward and backward waves [Eqs. (13) and (14)]

$$V(z=0) = V_{(f,0,z=0)}(1 + \Gamma_\ell e^{-2\gamma\ell}) \sum_{i=0}^{n-1} (\Gamma_0\Gamma_\ell e^{-2\gamma\ell})^i. \quad (15)$$

Similarly, the voltage at $z=l$ is

$$V(z=l) = V_{(f,0,z=0)}(1 + \Gamma_\ell) e^{-\gamma\ell} \sum_{i=0}^{n-1} (\Gamma_0\Gamma_\ell e^{-2\gamma\ell})^i. \quad (16)$$

The currents $I(z=0)$ and $I(z=l)$ are obtained by replacing $V_{(f,0,z=0)}, \Gamma_\ell$ and Γ_0 with $I_{(f,0,z=0)}, -\Gamma_\ell$ and $-\Gamma_0$, respectively.²⁴ Expressions for the line impedance at $z=0$

and the voltage ratio between the ends of the transmission line follow:

$$Z(z=0) \equiv \frac{V(z=0)}{I(z=0)} = \frac{1 + \Gamma_\ell e^{-2\gamma\ell}}{1 - \Gamma_\ell e^{-2\gamma\ell}} Z_0, \quad (17)$$

$$T(z=0) \equiv \frac{V(z=\ell)}{V(z=0)} = \frac{(1 + \Gamma_\ell)e^{-\gamma\ell}}{1 + \Gamma_\ell e^{-2\gamma\ell}}. \quad (18)$$

The voltage transfer function between the voltage source and the end of the transmission line, $T_s = V(z=\ell)/V_s$, can be expressed

$$T_s = T_1 T_2; \quad T_1 = \frac{V_{(f,0,z=0)}}{V_s} \quad T_2 = \frac{V(z=\ell)}{V_{(f,0,z=0)}}, \quad (19)$$

where T_1 and T_2 are given by Eqs. (10) and (16), respectively. Substituting for T_1 and T_2 yields

$$\begin{aligned} T_s &\equiv \frac{V(z=\ell)}{V_s} = \frac{Z_0 \| Z_X}{Z_0 \| Z_X + Z_I} (1 + \Gamma_\ell) e^{-\gamma\ell} \sum_{i=0}^{n-1} (\Gamma_0 \Gamma_\ell e^{-2\gamma\ell})^i \\ &= \frac{Z_0 \| Z_X}{Z_0 \| Z_X + Z_I} \\ &\quad \times \frac{(1 + \Gamma_\ell)(1 - (\Gamma_0 \Gamma_\ell e^{-2\gamma\ell})^n) e^{-\gamma\ell}}{1 - \Gamma_0 \Gamma_\ell e^{-2\gamma\ell}}. \end{aligned} \quad (20)$$

Finally, the impedance seen by the network analyzer is, from Eq. (17)

$$\mathcal{Z} = Z_X \left\| \left(\frac{1 + \Gamma_\ell e^{-2\gamma\ell}}{1 - \Gamma_\ell e^{-2\gamma\ell}} Z_0 \right) \right. = \frac{Z_0 Z_X (1 + \Gamma_\ell e^{-2\gamma\ell})}{(Z_0 + Z_X) + (Z_0 - Z_X) \Gamma_\ell e^{-2\gamma\ell}}. \quad (21)$$

It should be noted that \mathcal{Z} is independent of Γ_0 , i.e., it is dependant on Z_X but independent of the network analyzer impedance.

We now turn attention to the case of a wave injected by the Mirnov coil, with $Z_I = \infty$, $|V_m| > 0$ (i.e., the network analyzer has been removed). The results of the previous case apply with the parameters $\{V_s, Z_I, Z_X, \Gamma_\ell, \Gamma_0\}$ replaced by $\{V_m, Z_s, Z_p, \Gamma_0, \Gamma_\ell\}$. From Eq. (20) the transfer function is therefore

$$\begin{aligned} \mathcal{T}_m &\equiv \frac{V(z=0)}{V_m} \\ &= \frac{Z_0 \| Z_p}{Z_0 \| Z_p + Z_s} \frac{(1 + \Gamma_0)(1 - (\Gamma_0 \Gamma_\ell e^{-2\gamma\ell})^n) e^{-\gamma\ell}}{1 - \Gamma_0 \Gamma_\ell e^{-2\gamma\ell}}. \end{aligned} \quad (22)$$

In the case that $\ell \ll 1/|\gamma|$, $\exp -\gamma\ell \approx 1$; with $|\Gamma_0 \Gamma_\ell| < 1$, Eqs. (20)–(22) reduce to

$$T_s = \frac{Z_p \| Z_s \| Z_X}{Z_p \| Z_s \| Z_X + Z_I}, \quad (23)$$

$$\mathcal{Z} = Z_p \| Z_s \| Z_X, \quad (24)$$

$$\mathcal{T}_m = \frac{Z_p \| Z_X}{Z_p \| Z_X + Z_s}. \quad (25)$$

That is, as expected, the effect of the transmission line is removed.

Taking the Taylor series expansion to first order in $\gamma\ell$ with $\mathcal{R} = \mathcal{G} = 0$, Eq. (21) becomes

$$\mathcal{Z} = Z_X \left\| \left(Z_p \| Z_s \| (Z_c - Z_0) + \frac{Z_0^2}{Z_p \| Z_s} \right) \frac{Z_0}{Z_c - Z_0} \right), \quad (26)$$

where

$$Z_c = \frac{1}{j\omega C\ell}. \quad (27)$$

In the limit $Z_c \gg 1$, the second term becomes insignificant and Eq. (26) reduces to

$$\mathcal{Z} \approx Z_X \| Z_p \| Z_s \| Z_c, \quad (28)$$

i.e., the effect of the transmission line reduces to an additional parallel capacitance. This is the limit considered by Lovberg.¹⁴

A more interesting situation results if, during the determination of impedance by the network analyzer, the value of the impedance Z_X is adjusted to have a value $Z_X \| Z_I$ where Z_I is here taken to be the impedance of the digitizer. That is, with $Z_X \rightarrow Z_X \| Z_I$, Eq. (21) can be written

$$\mathcal{Z} = \frac{Z_0(1 + \Gamma_0)(1 + \Gamma_\ell e^{-2\gamma\ell})}{2(1 - \Gamma_0 \Gamma_\ell e^{-2\gamma\ell})} \quad (29)$$

and Eqs. (22) [assuming finite dissipation and $n \rightarrow \infty$ so that $(\Gamma_0 \Gamma_\ell e^{-2\gamma\ell})^n = 0$] and (29) can be expressed as

$$\mathcal{T}_m = \frac{1}{D}, \quad (30)$$

$$\mathcal{Z} = \frac{N}{D}, \quad (31)$$

where

$$N = \frac{1}{2}(A_+ + A_-), \quad (32)$$

$$D = \frac{A_+ - \Gamma_0 A_-}{Z_0(1 + \Gamma_0)}, \quad (33)$$

$$A_\pm = [Z_s \pm Z_0(1 + Z_s/Z_p)] e^{\pm\gamma\ell}. \quad (34)$$

The numerical method of Heeter *et al.* described in Sec. III, which is based on a lumped circuit model, provides extraction of the transfer function \mathcal{T}_m from a rational polynomial fit to \mathcal{Z} with real coefficients in powers of s , i.e., N and D are expressed in the form

$$N = \sum_{i=0}^n a_i s^i \quad (35)$$

$$D = \sum_{i=0}^n b_i s^i \quad (36)$$

in which $s = j\omega$, the a_i and b_i coefficients are real, and the series is finite. Below we show that the lumped-circuit model is valid in the case of a lossy but distortionless transmission line (i.e., the line exhibits no dispersion) terminated at $z=0$ by a real impedance. The condition for a transmission line to be distortionless is²⁹

$$\frac{\mathcal{R}}{\mathcal{L}} = \frac{\mathcal{G}}{C} \quad (37)$$

so that

$$Z_0 = \sqrt{\mathcal{L}\mathcal{C}}, \quad (38)$$

$$\gamma = \sqrt{\mathcal{R}\mathcal{G}} + s\sqrt{\mathcal{L}\mathcal{C}}, \quad (39)$$

$$v_{\text{phase}} = 1/\sqrt{\mathcal{L}\mathcal{C}}. \quad (40)$$

Recalling that $Z_p = 1/sC_p$, $Z_s = R_p + sL_p$, we note that the coefficients multiplying $e^{+\gamma\ell}$ and $e^{-\gamma\ell}$ in Eq. (34) are polynomials in s with positive integer exponents. As the input termination and Z_0 are both real, Γ_0 is real. The term $e^{\pm\gamma\ell}$ can be expanded as

$$e^{\pm\gamma\ell} = e^{\pm\ell\sqrt{\mathcal{R}\mathcal{G}}} \left(1 \pm s\ell\sqrt{\mathcal{L}\mathcal{C}} + \dots + \frac{(\pm s\ell\sqrt{\mathcal{L}\mathcal{C}})^{(n-1)}}{(n-1)!} + R_n(s) \right), \quad (41)$$

where

$$R_n(s) = \frac{(\pm s\ell\sqrt{\mathcal{L}\mathcal{C}})^n}{n!} e^{\pm\xi} \quad (42)$$

is the Lagrangian form of the remainder,³⁰ and $0 \leq |\xi| \leq s\ell\sqrt{\mathcal{L}\mathcal{C}}$. The effect of truncating the series at a finite n is to introduce errors of order $|R_n(s)|/|e^{j\omega\ell\sqrt{\mathcal{L}\mathcal{C}}}| = |R_n(s)|$ into $|e^{\gamma\ell}|$, and hence the expressions for N and D . In the limit $n \rightarrow \infty$, $R_n(s) \rightarrow 0$, and so a rational polynomial of finite, but arbitrarily large order will contribute a vanishing error to N and D .

Thus we have shown that expressions for N and D are reducible to the polynomial forms shown in Eqs. (35) and (36) providing that the line is distortionless and the terminating impedance at $z=0$ is real. Physically, this implies that the attenuation and phase speed of an injected signal is independent of its frequency. The required frequency independence arises because in the lumped-circuit model every injected frequency appears instantly at the output.

Before discussing the lumped-circuit model any further, particularly in relation to providing a technique to extract the transfer function \mathcal{T}_m from measurements of \mathcal{Z} , the special case of $D=0$, corresponding to a resonance condition on \mathcal{Z} , warrants comment. In the case that the transmission line and Mirnov probe are lossless ($\mathcal{R} \rightarrow 0, \mathcal{G} \rightarrow 0, R_p \rightarrow 0$) and $\Gamma_0=1$, the resonant condition may be expressed

$$\frac{\ell}{\lambda} = \frac{1}{2\pi} \tan^{-1} \left[\frac{Z_0(1 - \omega^2 L_p C_p)}{\omega L_p} \right], \quad (43)$$

where $\lambda = 2\pi/(\omega\sqrt{\mathcal{L}\mathcal{C}})$ is the wavelength of the signal in the transmission line. For frequencies well below the first self-resonant frequency (i.e., $\omega \ll 1/\sqrt{L_p C_p}$) Eq. (43) becomes

$$\frac{\ell}{\lambda} = \frac{1}{2\pi} \tan^{-1} \left(\frac{Z_0}{\omega L_p} \right), \quad \omega \ll \frac{1}{\sqrt{L_p C_p}}. \quad (44)$$

The above relations are useful for obtaining the line lengths at which resonances occur for a given frequency. For $\ell/\lambda \ll 1$ the frequency of the lowest resonance is obtained by a Taylor expansion of Eq. (43)

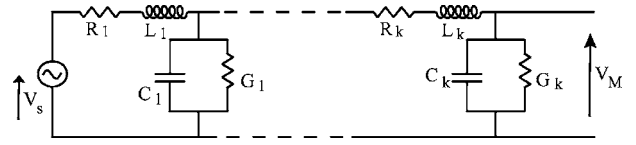


FIG. 4. A k th order lumped-circuit representation of the Mirnov coil and line sections proposed by Heeter *et al.* The voltage source V_s represents the Mirnov coil induced signal; V_M is the signal at the digitizer.

$$\omega = \frac{1}{\sqrt{L_p(C_p + \mathcal{C}\ell)}}. \quad (45)$$

It is seen that the effect of the transmission line is to down-shift the resonance of the Mirnov coil from its value in the absence of the transmission line. For $C_p \ll \mathcal{C}\ell$ the resonance is between the probe inductance and line capacitance as recognized by Lovberg.¹⁴ Finally, from Eqs. (44) and (45) in the limit $C_p \ll \mathcal{C}\ell$,

$$\frac{\ell}{\lambda} = \frac{1}{2\pi} \tan^{-1} \sqrt{\frac{\mathcal{L}\ell}{L_p}} \quad (46)$$

from which it can be seen that line resonances with $\ell/\lambda \ll 1$ occur with $L_p \geq \mathcal{C}\ell$.

In summary, comparison of \mathcal{Z} and \mathcal{T}_m reveals that extraction of $\mathcal{T}_m = 1/D$ from $\mathcal{Z} = N/D$ is valid provided (i) the transmission line exhibits no dispersion and is terminated at $z=0$ by a real impedance, and (ii) during the determination of \mathcal{Z} , Z_X is adjusted to have a value $Z_X|Z_I$ with Z_I taken to be the impedance of the digitizer. This result is valid for arbitrary boundary conditions at $z=0$ (i.e., there are no restrictions on the choice of Z_I and Z_X). However, unless $\Gamma_0=0$ line resonances will be present and, depending on the choice of terminations, these may occur well below the first self-resonant frequency.

III. LUMPED-CIRCUIT MODEL

Analysis of the transmission line is considerably simplified if propagation delays are neglected. This was the approach of Heeter *et al.* who modeled the circuit of serially connected transmission lines shown in Fig. 1 by the lumped-circuit shown in Fig. 4 consisting of k T -model circuit elements. The circuit impedance at the digitizer end of the circuit can be written as the rational function $Z_k(s) = N_k(s)/D_k(s)$ where $N_k = \sum_{i=0}^{m-1} a_i s^i$ and $D_k = \sum_{i=0}^m b_i s^i$ are polynomials in the Laplace transform s . Here, $m=2k$ is the number of poles in a k th order lumped circuit. The functions N_k and D_k are constructed by the recurrence relations

$$N_{k+1} = N_k + D_k Y_{k+1}, \quad (47)$$

$$D_{k+1} = D_k + X_{k+1} N_{k+1}, \quad (48)$$

where $X_k = G_k + C_k s$ and $Y_k = R_k + L_k s$; the transfer function for k stages is always given by $H_k = 1/D_k$. If Z_k is expressed in this form, Heeter *et al.* showed that the transfer function, $H_k = V_M/V_s$, is trivially obtained as $H_k = 1/D_k$. This is a useful relation as it suggests a means of obtaining the transfer function simply by measuring the circuit characteristics from one end of the transmission line.

TABLE I. Initial values of circuit components and computed values for lumped circuits with $k=1$, $k=2$, $k=3$.

	Exact	$k=1$	$k=2$	$k=3$
$R_1(\Omega)$	15	82.1	15.0	-2.30
$L_1(\text{mH})$	1	2.31	1.00	0.02
$C_1(\text{nF})$	50	1.03	50.0	224.0
$G_1(m\Omega^{-1})$	1.5	0.97	1.50	401.0
$R_2(\Omega)$	5		5.01	16.91
$L_2(\text{mH})$	2.5		2.50	-0.02
$C_2(\text{nF})$	1		1.00	-3.71
$G_2(m\Omega^{-1})$	1		1.00	-48.6
$R_3(m\Omega)$				27.66
$L_3(\text{mH})$				2.50
$C_3(\text{nF})$				1.00
$G_3(m\Omega^{-1})$				1.00

There are various techniques for obtaining a rational function fit to a given data set. Perhaps the simplest is the Padé rational approximation. A requirement here is that the data can be represented by a Taylor series expansion with coefficients of the rational function matched to the derivative at the expansion point. The question of uniqueness was addressed by Walsh^{31,32} who showed that the requirement is that (a) N_k and D_k have no common zeros and (b) a normalization condition must be imposed. The normalization chosen by Heeter *et al.* is $b_0=1$. Like Taylor's series, the accuracy of Padé approximations usually decreases rapidly away from the expansion point. Other algorithms such as that used by MATLAB³³ minimize the weighted sum of squared errors at multiple data points (i.e., the error is minimized over a range of frequencies). The issue of uniqueness in this case is yet to be addressed.

It is instructive to write down the general form of the b_0 term

$$\begin{aligned}
b_0 = 1 + & \prod_{i=1}^k R_i G_i + \Lambda(k-2) \sum_{i_1=1}^k \sum_{i_2=i_1}^k R_{i_1} G_{i_2} \\
& + \Lambda(k-3) \sum_{i_1=1}^{k-1} \sum_{i_2=i_1}^{k-1} \sum_{i_3=i_2+1}^k \sum_{i_4=i_3}^k R_{i_1} G_{i_2} R_{i_3} G_{i_4} \\
& + \Lambda(k-4) \sum_{i_1=1}^{k-2} \sum_{i_2=i_1}^{k-2} \sum_{i_3=i_2+1}^{k-1} \sum_{i_4=i_3}^k \sum_{i_5=i_4+1}^k R_{i_1} G_{i_2} \\
& \times R_{i_3} G_{i_4} R_{i_5} G_{i_6} + \dots, \quad (49)
\end{aligned}$$

where $\Lambda(k-j)=1$ for $k \geq j$ and is otherwise zero. The case $b_0=1$ can be seen to represent the limit when $R_k=0$ and/or $G_k=0$. It is often the case that the finite series resistance must be retained (i.e., $R_k \neq 0$) but that G_k can be neglected in which case taking $b_0=1$ is reasonable. This is presumably true for the JET probe systems considered by Heeter *et al.*

The procedure carried out by Heeter *et al.* is to obtain a rational function fit to the data, to apply the normalization $b_0=1$, and hence the transfer function H_k . In the general case when $R_k \neq 0$ and $G_k \neq 0$ it is necessary to compute b_0 explicitly. This is not straightforward and there are at least three possible approaches that can be used to obtain H_k given Z_{meas} :

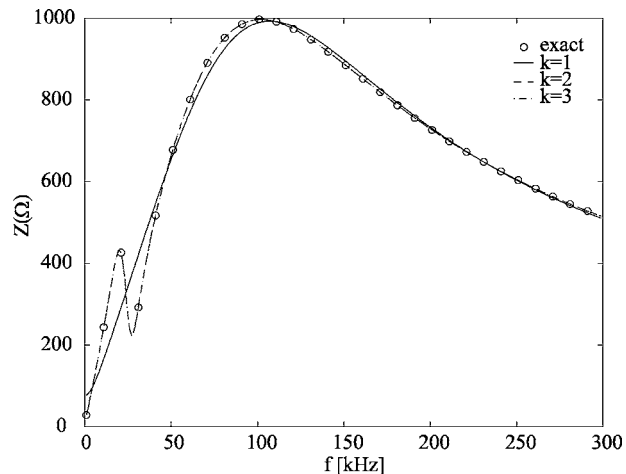


FIG. 5. Rational function fits of Z_{meas} compared to the exact values (indicated by circles). The cases $k=2$ and $k=3$ overlay.

- generate expressions for the coefficients of the polynomials N_k and D_k in terms of the circuit components, and vary the circuit component to obtain a least squares fit to Z_{meas} ;
- generate a rational function in terms of the set of variables X_k and Y_k using the recurrence relations (47) and (48) and vary X_k and Y_k to obtain the least squares fit to Z_{meas} ;
- directly perform a least squares fit to Z_{meas} with a rational function $N_{\text{fit}}/D_{\text{fit}}$ of undetermined and independent coefficients (the method of **unconstrained fit**), and then eliminate the free multiplicative constant χ present in the ratio $Z_k=N_{\text{fit}}/D_{\text{fit}}=(N_k\chi)/(D_k\chi)$ to extract $H_k=1/D_k$.

Methods (a) and (b) are equivalent, and involve solving for all $4k$ circuit components. In method (c), the elimination of χ will also be, in general, equivalent to solving the equations $N_{\text{fit}}=N_k$ and $D_{\text{fit}}=D_k$ for all circuit components. As such, the complexity of the third method is equivalent to (a) and (b). In every case at least some if not all of the circuit components need to be extracted to determine the transfer function uniquely.

Finally, the transfer function is obtained for a second order circuit with component values given in Table I using the method of unconstrained fit with a simulated impedance characteristic. The details of the procedure are contained in the Appendix. Figure 5 shows the fit to a rational function using the MATLAB `invfreqs` routine with $k=1$, $k=2$ and $k=3$, respectively. Not unexpectedly, the fits to Z_{meas} for $k=2$, $k=3$ overlay the original values Z_{meas} , whereas the fit for $k=1$ is poor. The computed circuit components are listed in Table I. Only in the case $k=2$ does the method successfully recover all the circuit component values, and there are large errors in the other cases. For $k=3$ several of the circuit components are active suggesting the presence of voltage sources within the network. Figure 6 shows the computed function H_k for each case together with the exact value of the transfer function, H_s . In the case $k=2$ H_k overlays H_s ; however, in the other cases there are large discrepancies. For example, with $k=1$, a significant feature around 20 kHz is not repre-

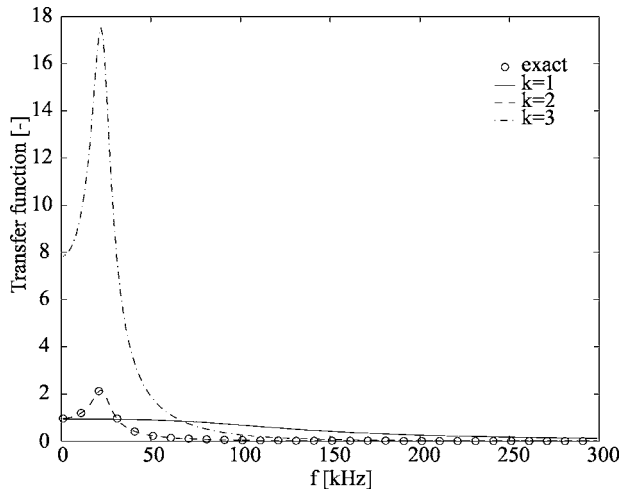


FIG. 6. Computed transfer function H_k for $k=1$, $k=2$ and $k=3$ with exact values, H_s , indicated.

sented, whereas for $k=3$, the magnitude of the computed transfer function is too large by a factor of ~ 10 . Thus, although rational functions corresponding to both the $k=2$ and $k=3$ lumped circuits provide good fits to Z_{meas} , only the $k=2$ case provides an accurate calculation of H_s .

These results show that the MATLAB `invfreqs` routine does not always provide a unique rational function approximation and there may exist multiple rational functions that can fit the data to the tolerance of the data, each yielding a different H_k . More generally, H_k appears to converge with an increasing number of passive circuit components, up to the order of the circuit under test but diverges once active components are found. Notwithstanding these limitations, when performed carefully, the use of the method of unconstrained fit, together with the elimination of the free multiplicative constant, is a useful tool with which to extract the voltage transfer function in established systems.

IV. COMPARISON OF THE LUMPED-CIRCUIT MODEL WITH THE TRANSMISSION LINE MODEL

In this section we examine the accuracy of the lumped-circuit model when transmission line effects are included. Two examples are considered, both lossless transmission lines terminated with an open circuit at $z=0$ (i.e., $\Gamma_0=1$). These conditions were examined in Sec. II where it was shown that for these conditions $Z(s)$ can be expressed as a rational function, and T_m by its denominator [i.e., the same form as for the variables $Z(s)$ and H_k defined in Sec. III]. Since the coefficients of the rational functions representing $Z(s)$ are infinite series, the success of the lumped-circuit model will depend on the rate of decay of successive terms. Generally, the larger the number of terms in the rational polynomial Z_s , the larger the number of T -model circuits that will need to be used in the lumped-circuit model which will increase the likelihood that the extracted transfer function will be in error.

In the first example, we consider the properties of a lossless system in which transmission line effects are small and good agreement would be anticipated using only a few T -model circuits. Using parameters, $L_p=R_p=0$, \mathcal{L}

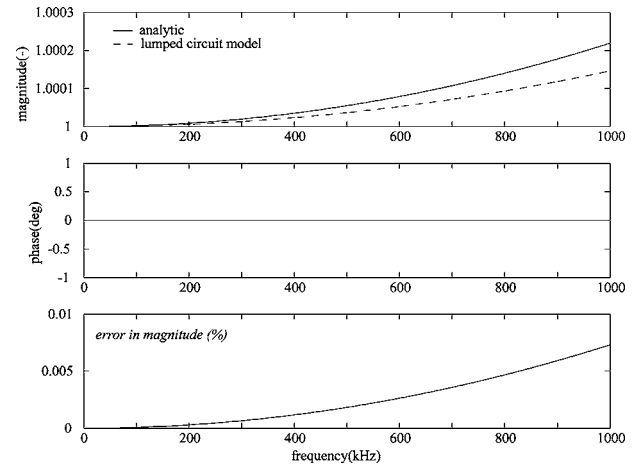


FIG. 7. Transfer function computed for a lossless line with $\Gamma_0=1$, $Z_s=0$, $Z_0=50 \Omega$, $C=66.6 \text{ pF/m}$, $\mathcal{L}=166.6 \text{ nH/m}$ and $\ell=1 \text{ m}$ using one T -model circuit.

$=166 \text{ nH/m}$, $C=66.6 \text{ pF/m}$, and $\ell=1 \text{ m}$, expressions for $T_m(s)$ and $Z(s)$ [from Eqs. (32) and (33) with $Z_s=0$] are particularly simple:

$$T_m(s) = 1/D(s), \quad (50)$$

$$Z(s) = N(s)/D(s), \quad (51)$$

where

$$N = \sqrt{\frac{\mathcal{L}}{C}} \sinh \ell \sqrt{\mathcal{L}Cs} = \mathcal{L}\ell s + \frac{\mathcal{L}^2 C (\ell s)^3}{6} + \frac{\mathcal{L}^3 C^2 (\ell s)^5}{120} + O[s]^7, \quad (52)$$

$$D = \cosh \ell \sqrt{\mathcal{L}Cs} = 1 + \frac{(\ell \sqrt{\mathcal{L}Cs})^2}{2} + \frac{(\ell \sqrt{\mathcal{L}Cs})^4}{24} + O[s]^6. \quad (53)$$

Figure 7 compares the results of the lumped circuit model obtained using $k=1$ (i.e., one T -model circuit) with T_m given in Eq. (50). There is no discrepancy in phase between the two approaches and the discrepancy in the magnitude is less than 0.01%. The result for $k=2$ is shown in Fig. 8 and displays a spurious 180° shift around 650 kHz. The reason for the phase change is the existence of a common zero in $N(s)$ and $D(s)$.

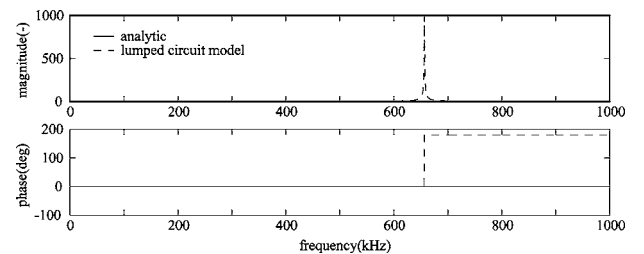


FIG. 8. Transfer function computed for a lossless line with $\Gamma_0=1$, $Z_s=0$, $Z_0=50 \Omega$, $C=66.6 \text{ pF/m}$, $\mathcal{L}=166.6 \text{ nH/m}$ and $\ell=1 \text{ m}$ using two T -model circuits.

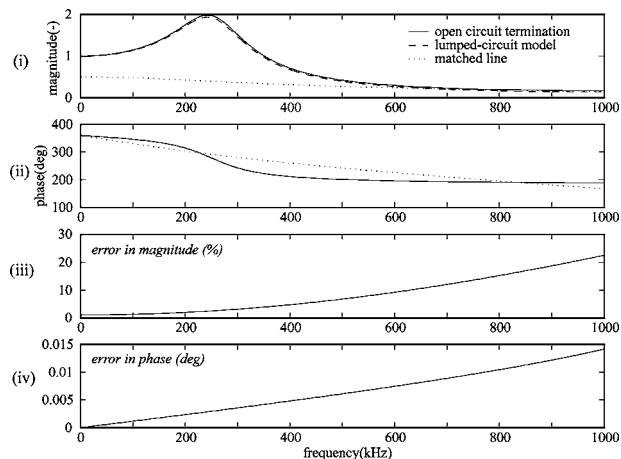


FIG. 9. Transfer function for a JET coil with open circuit ($\Gamma_0=1$) at $z=0$ computed using the lumped-circuit model with three T -model circuits and comparison with \mathcal{T}_m . In this case $R=0$, $G=0$, $Z_0=50 \Omega$, $C=66.6 \text{ pF/m}$ and $\mathcal{L}=166.6 \text{ nH/m}$. The dotted lines in (i) and (ii) are for a transmission line with matched line conditions at $z=0$ ($\Gamma_0=0$) computed using Eq. (30).

The second example examined is for a JET Mirnov coil based on parameters contained in Heeter *et al.*¹⁷ The details of the system examined are as follows. The cable has length $\ell=100 \text{ m}$ in which waves travel with phase velocity $v_{\text{phase}}=3 \times 10^8 \text{ m/s}$ (parameters given by Heeter *et al.*¹⁷). For the cable characteristics not given in Heeter *et al.*¹⁷ the following are assumed: $\mathcal{R}=\mathcal{G}=0$ and $Z_0=50 \Omega$ giving $C=1/(Z_0 v_{\text{phase}})=66.6 \text{ pF/m}$. For the Mirnov probe, $L_p=50 \mu\text{H}$ and $R_p=50 \Omega$ (values given by Heeter *et al.*¹⁷). The value of the stray capacitance C_p is not given by Heeter *et al.*¹⁷ so a value of 10 pF is assumed, putting the coil self-resonant frequency above 7 MHz . The input impedance of the JET digitizer is $10 \text{ k}\Omega$. As this is very large compared to the line impedance, it will be neglected.

Figure 9 compares values of H_k and \mathcal{T}_m defined in Eqs. (30) and (33) for $k=3$ (i.e., three T -model circuits). Using $k=3$ provides the optimum physical solution; solutions with $k>3$ were discarded as they included active circuit components. The discrepancy in phase and magnitude increases monotonically and approximately quadratically with frequency reflecting the increasing importance of higher order terms. Although the phase discrepancy is remarkably small ($<0.015^\circ$ for frequencies up to $<1 \text{ MHz}$), the discrepancy in the magnitude is more significant: around 7% at 500 kHz and 22% at 1 MHz . An interesting feature seen in Fig. 9 is the rapid change in phase and peaking in the magnitude of \mathcal{T}_m around 250 kHz . The appearance suggests it is the location of a strongly damped resonance; application of Eq. (45) (which is strictly valid in the case of no dissipative elements) gives the resonant location at 275 kHz , close to the actual peak. The case where the line is terminated at the digitizer with a matching impedance is also shown in Fig. 9, evaluated from Eq. (22) with $n \rightarrow \infty$ and $\Gamma_0=0$. At this frequency, from Eq. (44), $\ell/\lambda=0.08$. It is seen that the resonance has now disappeared; however, at low frequencies the magnitude of \mathcal{T}_m has been reduced by a factor of 2.

The acceptable level of discrepancy between the lumped-circuit and transmission line models will depend on context. For example, a common requirement in nuclear fu-

tion research is to determine the spatial wavelength, and phase of a traveling sinusoidal fluctuation.³⁴ This requires phase information at multiple spatial locations with the fluctuation magnitude playing no role. If instead there are multiple sinusoidal fluctuations at a given frequency then the measured fluctuation amplitude is significant. For example, a recent algorithm developed by the authors to extract multiple modes at a given frequency employs both magnitude and phase.³⁴

In summary, using the approach of Heeter *et al.* to compute \mathcal{T}_m for a JET Mirnov coil yields discrepancies of $<0.015^\circ$ and $<22\%$ in the computed phase and magnitude, respectively, for frequencies up to 1 MHz and a discrepancy in the magnitude $<5\%$ for frequencies up to 500 kHz . The existence of a system resonance around 250 kHz has been identified and can be removed by correctly matching the line at $z=0$. Care should be taken in interpreting any computed singularities in \mathcal{T}_m which may be due to the form of the computed rational function introducing spurious resonances. Finally, as stated in Sec. II, in the case of $\Gamma_0 \neq 1$ it may not be possible to relate \mathcal{T}_m to the rational function representation of \mathcal{Z} , and in this case it would be anticipated that the discrepancy of the lumped-circuit approach may be significantly larger.

V. EXTENSION TO WAVES OF FINITE DURATION

The results presented in the previous section assumed Fourier-stationary conditions, namely, that a signal with constant amplitude and varying as $\exp j\omega t$ is injected from time $t=0$. The analysis takes into account the possibility that the injected wave will be reflected $n \rightarrow \infty$ times. However, in practice signals are of finite duration. The analysis of the general situation can be modeled by writing the injected voltage (and current) in the form

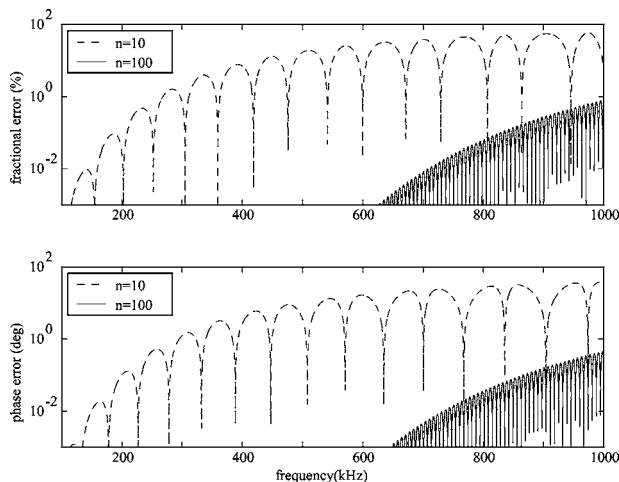
$$V = \sum_{i=1}^{\infty} \bar{V}_i \mathcal{H}(t - \alpha_i) \exp j(\omega t - \alpha_i), \quad (54)$$

where $\mathcal{H}(t - \alpha_i)$ takes the value 1 for $t > \alpha_i$ and is otherwise zero. In this treatment, however, once a signal appears it never disappears, but is instead nulled out by another signal injected at a later time. The time taken for the initial signal to effectively disappear depends on the damping of the system. Formal inclusion of all Fourier transients clearly adds another level of complexity. It is therefore of interest to understand when the steady-state approximation may be used.

Consider the time evolution of \mathcal{T}_m following the launch of a wave with constant frequency and amplitude at time $t=0$ and of duration ΔT . From Eq. (22) \mathcal{T}_m changes at discrete intervals of time

$$\Delta t = \frac{2\ell}{v_{\text{phase}}} = |2\gamma\ell/\omega|. \quad (55)$$

At time $t=\Delta T$ a Fourier-transient analysis would require two signals to be injected, one to null out the initial signal, and a second at the frequency and amplitude of the wave at this time. The discrepancy of the steady-state approximation may

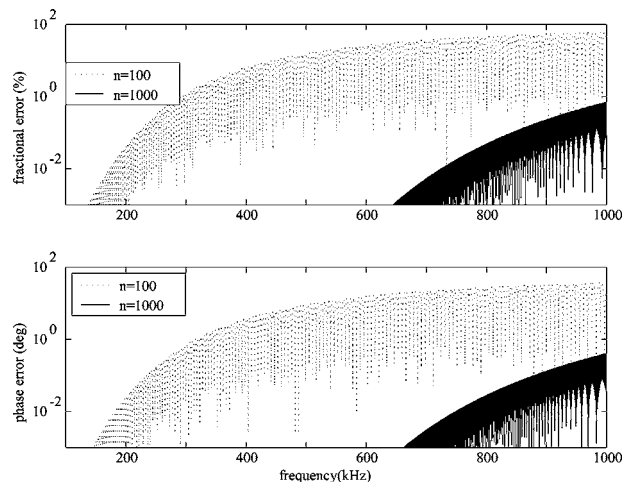
FIG. 10. Error in \mathcal{T}_m computed for a JET Mirnov coil with $R_p=50 \Omega$.

be characterized by the function $\epsilon = \mathcal{T}_m(n=\Delta T/\Delta t) - \mathcal{T}_m(n \rightarrow \infty)$ where $\mathcal{T}_m(n)$ denotes the value of \mathcal{T}_m after n reflections. Figure 10 plots the fractional discrepancy, $|\epsilon/\mathcal{T}_m(n=\infty)|$, and phase discrepancy, $\angle \epsilon$, for the JET Mirnov coil discussed in Sec. IV. The number of transits $n=1$ and $n=100$ correspond to $\Delta T=0.66 \mu\text{s}$ and $\Delta T=66 \mu\text{s}$, respectively. The envelope of the discrepancy increases with increasing frequency; for $\Delta T=66 \mu\text{s}$ the maximum discrepancy in the magnitude and phase of \mathcal{T}_m is 1% and 1° , respectively. For $\Delta T=133 \mu\text{s}$ these discrepancies decrease by nearly two orders. Figure 11 shows an identical calculation carried out for the same system but with R_p reduced to 5Ω . In this case, for a maximum discrepancy of 1% and 1° in the magnitude and phase, respectively, of \mathcal{T}_m , $n=1000$ corresponding to $\Delta T=660 \mu\text{s}$. This illustrates the important role of a dissipative element in reducing the time taken to reach Fourier-stationary conditions. Without Fourier-stationary conditions the lumped-circuit approach described in Sec. III cannot be used.

Finally, it is straightforward to apply the methodology described in this section to construct a function describing fractional discrepancies due to the assumption of Fourier-stationary conditions in terms of the duration and frequency of a fluctuation. This will make it possible via a look up table or similar means to ascertain with little effort whether the assumption of Fourier-stationary conditions is valid. Such a technique is currently under development.

VI. DISCUSSION

The main advantage of using a lumped-circuit model to represent a transmission line circuit is the possibility of being able to deduce the voltage transfer function directly from the electrical impedance measured from one end. This technique of ‘‘remote calibration’’ was first suggested and implemented by Heeter *et al.* In the present work we have extended the earlier work to enable the simultaneous inclusion of both serial resistance and parallel conductance elements in the transmission line network. Specifically, we have considered the case where b_0 , the first coefficient in the denominator of the rational function fit to Z [see Eq. (49)], is not unity. As in Heeter *et al.*,¹⁷ the rational function fit is obtained using MATLAB. In this work the symbolic processor Mathematica³⁵

FIG. 11. Discrepancy in \mathcal{T}_m computed for a JET Mirnov coil with $R_p=5 \Omega$.

is used to eliminate the free multiplicative constant. The case when $b_0=1$ (which arises, for example, when the admittance terms G_k can be neglected) is much simpler as the use of Mathematica is not required.

In this article we have formally proved that for the case of a lossy non-dispersive transmission line terminated with an arbitrary real impedance, \mathcal{T}_m may be extracted from the measurement of Z_m provided that during the determination of $\mathcal{Z}, \mathcal{Z}_X$ is adjusted to have a value $Z_X||Z_I$ with Z_I taken to be the impedance of the digitizer. This result extends the use of the lumped-circuit model of Heeter *et al.* beyond the case of an open-circuit termination.

Transient analyzes carried out have related the duration of a wave to the discrepancy in the magnitude and phase of the voltage transfer function using the steady-state approximation. In particular, for the JET Mirnov coil, the magnitude and phase of the transfer function can be determined to within 1% and 1° , respectively, for a wave of duration $66 \mu\text{s}$. Using a matched termination, waves will make only one pass down the transmission line before being completely damped, so the steady-state assumption is reached after only $0.66 \mu\text{s}$.

The most obvious application of the lumped-circuit approach, requiring no *a priori* information on the system, is for circuits terminated by an open circuit. In this case it has been demonstrated that the system is subject to a resonance which for the JET Mirnov coil is around 275 kHz. In contrast, employing a matched termination avoids all line resonances and optimizes the transient response, however, it requires the transmission line characteristics to be known in advance to enable line matching, possibly lessening the value of remote calibration. It should be noted that the JET coils exhibit significant temperature-dependent resistance which precludes using a matched termination at the digitizer.³⁶ Including resistive elements into the lumped-circuit model (if $R_k \neq 0$ and $G_k \neq 0$) adds considerably to the complexity of the lumped-circuit model since individual circuit elements must then be extracted.

Nevertheless, the results of the lumped-circuit approach for the extraction of the transfer function should be used with care. This is clear from the results of tests using data derived

from a two-stage T -model circuit showing that multiple rational functions may be generated that fit the measured impedance profile well, while yielding widely different transfer function characteristics. Many of these solutions contain unphysical active circuit components, and it is generally found the most accurate transfer function is obtained using the highest order rational function containing solely passive components. Applying the lumped-circuit model to a transmission line circuit, it has been shown that the lumped-circuit model can introduce spurious resonances due to the existence of a common zero in the numerator and denominator of the rational function fit to the impedance. With care, however, the lumped-circuit model has been successfully applied to obtain the transfer function of a JET Mirnov coil with the phase determined to within 0.1° for frequencies up to 1 MHz.

The work described in this article has been restricted to a single transmission line section connected to a Mirnov coil. In a practical system there may be multiple serially connected transmission line sections. For the design of a new diagnostic system it is preferable to minimize resonances by using matching terminations and choosing and constructing the voltage transfer function based upon expressions developed in this article and to reserve the lumped-circuit model for providing a check on data consistency.

ACKNOWLEDGMENTS

This work was funded jointly by the United Kingdom Engineering and Physical Sciences Research Council and by EURATOM. The authors would like to express their gratitude to the thoroughness and useful insights of the referee.

APPENDIX: CALCULATION OF THE TRANSFER FUNCTION, H_k

The method of **unconstrained fit** was employed in this work, due mainly to the availability of rational function fitting packages (e.g., MATLAB³³).

The procedure employed was as follows:

- (i) A rational function with denominator, D_{fit} , order k and numerator, N_{fit} , order $k-1$ was fitted to Z_{meas} . The value of k was assigned the value 2 in the initial pass and incrementally increased by 2 for each subsequent pass. In this work, the fit to the rational function was carried out by MATLAB, and normalized such that the coefficient of the leading power in D_{fit} was unity, so that $\chi=1/b_0$.
- (ii) With the aid of a symbolic processor (Mathematica³⁵), explicit functional forms for N_k and D_k were constructed using the recurrence relations (47) and (48), and normalized the way as in (i).
- (iii) Expressions for the normalized coefficients obtained in (ii) were equated to the fitted coefficients determined in (i) to obtain a set of linear equations which were solved to obtain values for the circuit components.
- (iv) Steps (i) to (iii) were repeated until any one of the extracted circuit components were active.
- (v) Using the largest set of physical (i.e., passive) circuit

components, the factor b_0 was calculated and the transfer function $H_k=1/D_k=\chi/D_{\text{fit}}$ determined.

Fitting of the transfer function and the extraction of circuit components was tested by generating the impedance profile for a known circuit. In each case the output circuit components were found to be equal to the test circuit to within numerical error.

- ¹C. Z. Cheng, L. Chen, and M. S. Chance, *Ann. Phys.* **161**, 21 (1984).
- ²C. Z. Cheng and M. S. Chance, *Phys. Fluids* **29**, 3695 (1986).
- ³R. Betti and J. P. Friedberg, *Phys. Fluids B* **3**, 1865 (1991).
- ⁴R. O. Dendy, C. N. Lashmore-Davies, and K. F. Kam, *Phys. Fluids B* **4**, 3996 (1992).
- ⁵N. N. Gorelekov, E. Fredrickson, E. Belova, C. Z. Cheng, D. Gates, S. Kaye, and R. White, *Nucl. Fusion* **43**, 228 (2003).
- ⁶A. Fasoli, J. B. Lister, S. E. Sharapov, S. Ali-Arshad, G. Bosia, D. Borba, D. J. Campbell, N. Deliyannis, J. A. Dobbins, C. Gormezano, H. A. Holties, G. T. A. Huysmans, J. Jacquinet, A. Jaun, W. Kerner, P. Lavanchy, J. M. Moret, L. Porte, A. Santagiustina, and L. Villard, *Nucl. Fusion* **35**, 1485 (1995).
- ⁷L. C. Appel, M. Hole, R. J. Akers, S. S. Pinches, and the MAST team, in *Proceedings of the Joint Lausanne-Varenna International, Workshop on Theory of Fusion Plasmas and Varenna*, 117 and *Società Italiana di Fisica and Bologna*, 2002.
- ⁸K. G. McClements, M. P. Gryaznevich, S. E. Sharapov, R. J. Akers, L. C. Appel, G. F. Counsell, C. M. Roach, and R. Majeski, *Plasma Phys. Controlled Fusion* **41**, 661 (1999).
- ⁹G. A. Cottrell, V. P. Bhatnagar, O. Da Costa, R. O. Dendy, J. Jacquinet, K. G. McClements, D. C. McCune, M. F. F. Nave, P. Smeulders, and D. F. H. Start, *Nucl. Fusion* **33**, 1365 (1993).
- ¹⁰E. D. Fredrickson, N. Gorelenkov, C. Z. Cheng, R. Bell, D. Darrow, D. Johnson, S. Kaye, B. LeBlanc, J. Menard, S. Kubota, and W. Peebles, *Phys. Rev. Lett.* **87**, 145001 (2001).
- ¹¹L. C. Appel, R. J. Akers, R. Martin, and T. Pinfold, 31st European Physical Society Conference on Plasma Physics, London, 28 June–2 July 2004 (P-4.195).
- ¹²I. H. Hutchinson, *Principles of Plasma Diagnostics* (CUP, Cambridge, 1987).
- ¹³J.-M. Moret, F. Buhlmann, D. Fasel, F. Hofmann, and G. Tonetti, *Rev. Sci. Instrum.* **69**, 2333 (1998).
- ¹⁴R. H. Lovberg, *Plasma Diagnostic Techniques*, edited by R. H. Huddleston and S. L. Leonard (Academic, New York, 1965), Chap. 3, p. 69.
- ¹⁵M. Tuszewski, *Rev. Sci. Instrum.* **61**, 2937 (1990).
- ¹⁶E. Fredrickson, K. M. McGuire, and Z. Y. Chang, *Rev. Sci. Instrum.* **66**, 813 (1995).
- ¹⁷R. F. Heeter, A. F. Fasoli, S. Ali-Arshad, and J. M. Moret, *Rev. Sci. Instrum.* **71**, 4092 (2000).
- ¹⁸*Measurement Techniques in Space Plasmas: Fields*, edited by R. F. Pfaff, J. E. Borovsky, and D. T. Young (American Geophysical Union, Washington, DC, 1998).
- ¹⁹M. K. Dougherty, N. Achilleos, N. Andre, C. S. Arridge, A. Balogh, C. Bertucci, M. E. Burton, S. W. H. Cowley, G. Erdos, G. Giampieri, K.-H. Glassmeier, K. K. Khurana, J. Leisner, F. M. Neubauer, C. T. Russel, E. J. Smith, D. J. Southwood, and B. T. Tsurutani, *Science* **307**, 1266 (2005).
- ²⁰K. Ostrikov, E. Tsakadze, S. Xu, S. V. Vladimirov, and R. Storer, *Phys. Plasmas* **10**, 1146 (2003).
- ²¹T. Vijayan, P. Roychowdhury, and N. Venkatramani, *J. Appl. Phys.* **96**, 4084 (2004).
- ²²U. Shumlak, B. A. Nelson, R. P. Golingo, S. L. Jackson, and E. A. Crawford, *Phys. Plasmas* **10**, 1683 (2003).
- ²³J. Wolowski, A. Kasprczuk, P. Parys, T. Pisarczyk, E. Woryna, and Yu P. Zakharov, *Plasma Phys. Controlled Fusion* **41**, A771 (1999).
- ²⁴N. N. Rao, *Elements of Engineering Electromagnetics* (Prentice-Hall, New York, 1977), p. 233.
- ²⁵W. R. Smythe, *Static and Dynamic Electricity* (McGraw-Hill, New York, 1950).
- ²⁶Rohde and Schwarz web site: <http://www.rsd.de>, 2005.
- ²⁷M. Hole and L. C. Appel, *IEE Proc.-Circuits, Devices and Systems* (accepted for publication).
- ²⁸L. M. Magid, *Electromagnetic Fields, Energy and Waves* (Wiley, London, 1972).

- ²⁹K. F. Sander and G. A. L. Reed, *Transmission and Propagation of Electromagnetic Waves* (CUP, Cambridge, 1978).
- ³⁰G. Arfken, *Mathematical Methods for Physicists*, 3rd ed. (Academic, Boston, 1985), p. 306.
- ³¹J. L. Walsh, *Trans. Am. Math. Soc.*, **33**, 668 (1931).
- ³²David M. Young and Robert Todd Gregory, *A Survey of Numerical Mathematics* (Addison–Wesley, Reading, MA, 1972), vol. 1.
- ³³MATLAB V6.0. The MathWorks, Inc., 2002.
- ³⁴M. J. Hole and L. C. Appel, 30th European Physical Society Conference on Controlled Fusion and Plasma Physics, St. Petersburg, 7–11 July 2003 (P-3.132).
- ³⁵S. Wolfram, *The Mathematica Book* (CUP, Cambridge, 2001).
- ³⁶S. Ali-Arshad (private communication).